Chimeric Capsid Protein as a Nanocarrier for siRNA Delivery: Stability and Cellular Uptake of Encapsulated siRNA

Kyung-mi Choi,[†,§] Seung-Hye Choi,[†,§] Hyesung Jeon,[†] In-San Kim,[‡] and Hyung Jun Ahn[†,*]

[†]Center for Theragnosis, Biomedical Research Institute, Korea Institute of Science and Technology, Seongbuk-Gu, Seoul 136-791, South Korea, and [‡]Department of Biochemistry and Cell Biology, Cell and Matrix Research Institute, School of Medicine, Kyungpook National University, Daegu 700-422, South Korea. [§]These authors contributed equally to this work.

ABSTRACT For the efficient cytoplasmic delivery of siRNA, we designed a chimeric capsid protein composed of a capsid shell, integrin targeting peptide, and p19 RNA binding protein. This recombinant protein assembled into a macromolecular container-like structure with capsid shell and provided a nanocarrier for siRNA delivery. Our capsid nanocarriers had dual affinity both for siRNA within the interior and integin receptors on the exterior, and the capsid shell structure allowed the encapsulated siRNAs to be protected from the external nucleases, leading to the enhanced stability of siRNA in serum conditions. The capsid nanocarriers could complex with siRNA in a size-dependent and sequence-independent manner and showed the pH-dependent complexing/dissocation behaviors with siRNA. Moreover, RGD peptides on the exterior surface of the capsid shell enabled the capsid nanocarriers to deliver siRNA into the cytosol of the target cells. Here, we demonstrated the superior efficiency of our siRNA/capsid nanocarrier complexes in RFP gene silencing, compared to untreated cells. These results provide an alternative approach to enhancing the stability of siRNA as well as to achieving targeted siRNA delivery.

KEYWORDS: capsid protein · siRNA delivery · nanocarrier · gene silencing · recombinant proteins

RNA interference (RNAi) is a highly conserved biological mechanism that uses small noncoding RNAs to silence gene expression. The endogenous small RNAs, called micro RNAs, are processed from hairpin precursors and regulate the important genes involved in cell death, differentiation, and development.[1] RNAi is fundamentally induced by 20- to 30-nucleotide double-stranded small interfering RNA (siRNA), which becomes incorporated with the RNA-induced silencing complex (RISC) and guides endonucleolytic cleavage of the complementary target mRNA.[2,3] RNAi has been of great interest not only as a powerful research tool to suppress the expression of a target gene but also as an emerging therapeutic strategy to silence disease genes.[4] However, the therapeutic applications of siRNA have been limited by its rapid enzymatic degradation and poor cellular uptake.[5,6] siRNA is quickly degraded by ribonucleases (RNases) activity in serum, and the anionic siRNA does not readily penetrate the cellular membranes by passive diffusion mechanisms.

To achieve the efficient cytoplasmic delivery of siRNA *in vitro* and *in vivo*, various siRNA delivery methods have been devised, including viral delivery systems, nonviral delivery systems (*e.g.*, liposomes or nanoparticles), and chemical modifications of siRNA.[7] The viral vectors delivering siRNA in the form of a viral genome have been shown to efficiently achieve gene silencing for an extended period,[8−12] but safety concerns such as the risk of mutagenesis and carcinogenesis and difficulties with large-scale manufacture may limit their use for siRNA delivery in clinical setting.[13,14] Nonviral gene delivery systems including lipid-based agents,[15,16] cationic polymers,[17,18] and cationic polypeptides[19−21] have been efficiently employed as the siRNA carriers as a result of their low immunogenicity, relatively low production cost, or reproducibility.[22,23] However, the dose-dependent toxicities found in the components of the carriers should be preferentially addressed for their *in vivo* applications. For example, polyethyleneimine and poly(L-lysine) have been shown to trigger necrosis and apoptosis in a variety of cell lines.[24,25] Also, chemically modified siRNA is known to have a greatly prolonged half-life in plasma,[26,27] but there are some potential risks that it may reduce RNAi efficiency[28] and also that its degradation may generate metabolites that might be unsafe or trigger unwanted effect.[7]

To overcome these limitations in siRNA delivery, we synthesized a nanocarrier for

* Address correspondence to hjahn@kist.re.kr.

Received for review July 12, 2011 and accepted October 10, 2011.

Published online October 10, 2011
10.1021/nn202597c

siRNA delivery by mimicking the gene delivery function of hepatitis B virus (HBV) capsid proteins. The resulting chimeric proteins, that is, capsid nanocarriers, are composed of a capsid shell, p19 RNA binding protein, and integrin-binding peptide (RGD peptide) and can assemble into a macromolecular container-like structure with a capsid shell. Depending on the complexing property of the p19 protein with siRNA, our chimeric capsid proteins bind dsRNA in a size-dependent and sequence-independent manner but do not bind ssRNA or dsDNA. In particular, one capsid nanocarrier allows about 120 p19 protein molecules to be located in the interior cavity of the capsid shell and thus drives the siRNA molecules to be encapsulated within the capsid shell. Consequently, the encapsulated siRNAs are protected from the nucleases present in serum and their stability is greatly enhanced. Moreover, the RGD peptides multivalently exposed on the exterior surface of the capsid shell can target tumor vasculature expressing $\alpha_v\beta_3$ intergrin[29] and thus allow the encapsulated siRNA to be efficiently delivered to the cytosol of cancer cells. The cellular uptake of our capsid nanocarriers was investigated by competition experiment and endocytic inhibitor studies, and the efficiency of siRNA/capsid nanocarrier complexes for siRNA delivery was confirmed through *in vitro* red fluorescent protein (RFP) gene silencing.

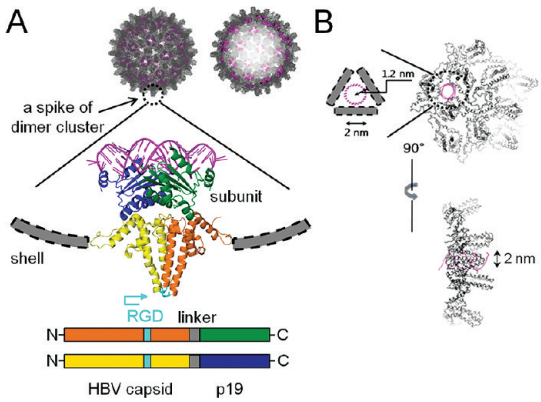

Figure 1. Three-dimensional structure of a chimeric capsid protein nanocarrier for siRNA delivery. (A) As a result of structural simulation, te siRNA/capsid nanocarrier complex is drawn in molecular structure. A dimer cluster is magnified to show a chimeric capsid-p19 fusion protein structure. A schematic diagram at the bottom explains how each component is connected to the other in a monomer. siRNA is colored magenta, and each color of the molecular structure corresponds to that of the schematic diagram. In addition to the exterior surface, the interior of the siRNA/capsid nanocarrier complex is also shown to depict encapsulated siRNAs. (B) Part of the shell surface is viewed down a local 3-fold axis. Three neighboring dimers with the relation of 3-fold symmetry form a channel to penetrate the shell surface, and these channels allow siRNAs to go in and out the shell surface. The molecular structures were prepared by the Pymol program, and the structures of HBV capsid protein and siRNA/p19 RNA binding protein complex are from the Protein Data Bank (PDB IDs: 1QGT, 1RPU).

RESULTS AND DISCUSSION

To design an efficient siRNA carrier, we modified the HBV capsid protein, which was previously reported to be a robust platform for genetic and chemical manipulation.[30,31] The electron microscopy analysis shows that a single HBV capsid protein truncated after residue 149 forms a shell particle that contains 240 subunits and has an overall diameter of 36 nm.[30] The dimer clustering of the subunits produces spikes on the surface of the shell particle and the surface-exposed spike tip corresponds to the loop segment consisting of the residues from D78 to D83 of the capsid protein. For precise targeting, we replaced A80 and S81 in the loop segment with the RGD peptides (CDCRGDCFC) to multivalently expose them on the shell surface of the synthesized chmeric nanoparticles (Figure 1A).

To incorporate the molecule(s) of interest into the designed carrier, we genetically added the p19 RNA binding protein to the C-terminus of the truncated HBV capsid subunit protein. p19 proteins from many viruses are known to function as a viral suppressor of RNA interference, and they recognize siRNA in a sequence-independent manner because direct and water-mediated intermolecular contacts are restricted to the backbone phosphates and sugar 2′−-OH groups of siRNA.[32,33] Since the p19 proteins form a homodimer with a concave surface made of eight β-strands in the middle of the dimer, each p19 dimer specifically binds double-stranded siRNA with nanomolar affinity, especially binding double-stranded 21-bp RNA with a 2-base overhang and a 5′ phosphate most efficiently. The 3D structural simulation using the Pymol program showed that a 31-amino-acid linker peptide inserted between the capsid subunit protein and p19 protein allows the p19 proteins to form the dimer in the interior cavity of the capsid (Figure 1A). Theoretically, one capsid shell could accommodate 120 p19 protein molecules. The capsid shell is fenestrated by the channels along a local 3-fold axis on the exterior (Figure 1B), and these channels were reported to allow accessibility of deoxynucleotides to the capsid interior.[34] Notably, our simulation results also showed that double-stranded siRNA molecules with a size range of 20−30 nucleotides could pass through the channels and reach the interior of the capsid shell.

The high affinity of p19 proteins for siRNA allows the capsid nanocarriers to form the siRNA/capsid nanocarrier (siRNA/CN) complexes, an important prerequisite for siRNA delivery. In the determination of the quantitative molar ratio between the bound siRNA and capsid nanocarrier, the relatively low concentration of capsid nanocarriers showed that the majority of siRNA molecules appeared in the unbound form at the lower band on a gel (Figure 2A). However, when the capsid nanocarriers' concentration was increased relative to the fixed amount of siRNA for each lane, the amount of the complexed siRNA proportionally increased, resulting

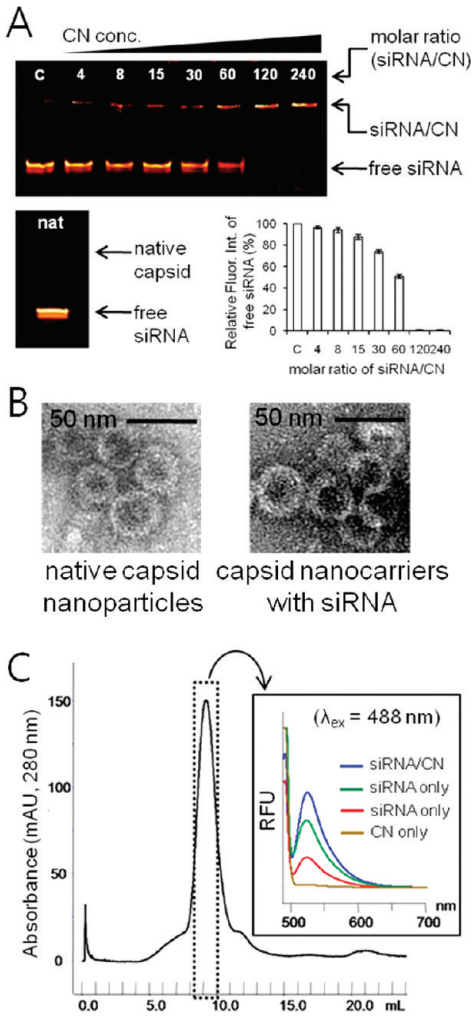

Figure 2. (A) Complexing of capsid nanocarriers with siRNA at various molar ratios. FITC-labeled siRNA (20 μg) in RNase-free distilled water was complexed with various amounts of capsid nanocarriers, at a molar ratio from 4 to 240 (siRNA per capsid nanocarrier), and then a gel retardation assay was performed; the amount of siRNA is kept constant for each lane, while that of CN is increasing from left to right. The native capsid protein did not complex with the FITC-labeled siRNA at a molar ratio of 120 (siRNA per capsid particle). For quantitative analysis, the fluorescence intensities of the uncomplexed siRNA bands on a gel were measured by Kodak Image Station, and each was corrected relative to the value obtained from the control. Results are presented as mean ± SE (n = 5). This result shows the quantitative molar ratio between the bound siRNA and capsid nanocarriers. Results are presented as mean ± SE (n = 5). (B) Transmission electron microscopy images of the empty native HBV capsid nanoparticles and siRNA/CN complexes. The molar ratio (siRNA to CN) of the siRNA/CN complexes was 120. Negative staining was performed using a droplet of a 2 wt % aqueous uranyl acetate solution. (C) Size exclusion chromatography elution profile of FITC-siRNA/CN complexes was monitored using UV absorbance at 280 nm, and subsequently emission spectra of the highlighted fractions were scanned at a fixed excitation wavelength (λ_{ex} = 488) by fluorescence spectrophotometer (blue line in the right panel). As a positive control, the emission spectra of uncomplexed FITC-labeled siRNA were obtained at two different concentrations (green and red line). For comparison, the emission spectrum of the uncomplexed capsid nanocarriers with the equal protein concentration was scanned at λ_{ex} = 488 (brown line).

in the shifted siRNA bands. Over a certain concentration of the capsid nanocarrier, the uncomplexed free siRNA was not seen on a gel anymore. From these studies, we could determine the maximum molar ratio between the bound siRNA and capsid nanocarrier as 120, that is, approximately 120 siRNA molecules can complex with one capsid nanocarrier. These results coincided with the theoretical molar ratio expected from the simulated structure of the capsid nanocarrier. The native capsid particles as a control sample did not complex with siRNA, and these results indicate that because the bacterially originated RNA in the cultured *E. coli* might already occupy the interior of the capsid, the FITC-labeled siRNA cannot associate with the capsid.

According to transmission electron microscopy (TEM) image analysis, the truncated HBV capsid particles and the siRNA/CN complexes formed spherical nanoparticles with average diameters of 36 ± 0.8 and 36 ± 0.4 nm [mean ± SD], respectively (Figure 2B). Similarly, dynamic light scattering analysis showed that the truncated HBV capsid particles and siRNA/CN complexes had average diameters of 37 ± 0.5 and 36 ± 0.8 nm [mean ± SD], respectively. Also, the size exclusion chromatography (SEC) analysis supported that the siRNA/CN complexes assemble into the capsid structures, because their elution volume (approximately 9 mL) coincided with that of the assembled native capsid structure (approximately 9 mL) (Figure 2C). Moreover, when the FITC-labeled siRNA was used to complex with the capsid nanocarriers, the peak fractions of the SEC chromatogram showed representative emission spectra of the FITC fluorophore on the fluorescence spectrophotometer (λ_{ex} = 488) (Figure 2C), whereas the uncomplexed capsid nanocarriers did not show such emission spectra. Taken together, these results indicate that the HBV capsid-derived nanocarriers expressed in the *E. coli* system assemble into the capsid architecture and these capsid nanocarriers can encapsulate siRNA into their interior. Moreover, the siRNA binding to capsid nanocarriers did not change either particle shape or particle size when compared to the native particles. In addition, by isolating siRNA from the siRNA/CN complexes present in the peak fractions of the SEC chromatogram, the amount of siRNA in the interior of the capsid nanocarriers could be measured by spectrophotometry (260 nm). These results also show that approximately 120 siRNA molecules are in the interior of one capsid nanocarrier.

When considering the efficient RNAi *in vivo* by delivering exogenous siRNA, the naked siRNA is relatively unstable in its native form and especially in blood because it is rapidly cleared *via* degradation by RNases.[35] To test the stability of the encapsulated siRNA against RNases, free siRNA and siRNA/CN complexes were incubated with RNases present in 50% fetal bovine serum (FBS). The free siRNA was fully degraded within 1 h, but the siRNA/CN complexes showed a distinguishable protecting effect against the RNases (Figure 3A).

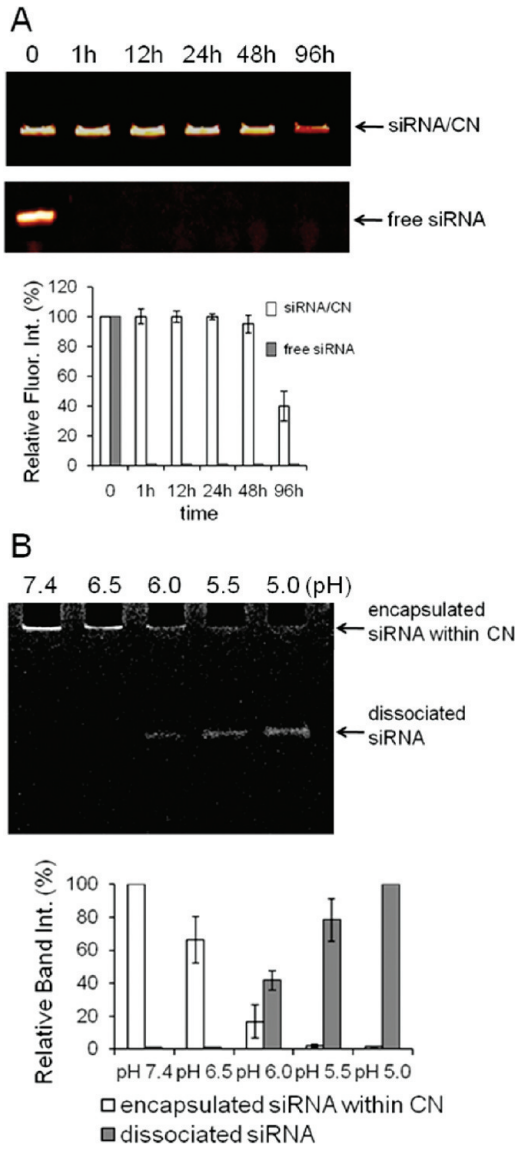

Figure 3. (A) Stability test of free siRNA and siRNA/CN complexes in serum conditions. The free siRNA and siRNA/CN complexes were incubated in 50% FBS solution (pH 7.4) for the indicated times and then analyzed by the gel retardation assay. Prior to incubation in serum conditions, each sample were incubated in PBS buffer (pH 7.4) for 15 min at room temperature. FITC-labeled siRNAs were used to enhance a detection limit, and their fluorescent images were obtained by Kodak Image Station. Results are presented as mean ± SE (n = 5). (B) pH effect on siRNA−capsid nanocarrier interaction. The capsid nanocarriers show pH-dependent complexing/dissociation behaviors with siRNA. In the various pH conditions, dissociation of siRNA from the siRNA/CN complexes was examined by gel electrophoresis. The encapsulated or dissociated siRNA was visualized by EtBr staining under UV light, and the resulting band intensities were quantified by Minibis Bioimaging system. Results are presented as mean ± SE (n = 5).

This enhanced stability of siRNA was expected to be derived from the capsid's shell structure surrounding the siRNAs, because the shielding effect does not allow access by RNases to the encapsulated siRNAs.

The binding affinity of capsid nanocarriers for siRNA was investigated in various pH conditions, because the gene delivery systems usually utilize the acidic environment of endosomal or lysosomal compartments for the cytosolic release of the cargo gene.[36] At neutral pH (7.4), most capsid nanocarriers had complexing capability with the siRNAs (Figure 3B). However, in the acidic condition at pH 6.5, the bound siRNAs began to dissociate from the capsid nanocarriers, and in more acidic condition (pH 5.5), more than half of the bound siRNAs were released from the capsid nanocarriers. When the acidity of the solution shifted to pH 5.0, the majority of siRNAs were dissociated from the capsid nanocarriers. These results indicate that the pH drop inside the endosome or lysosome vesicles may lower the binding affinity of capsid nanocarrier for siRNA and facilitate the cytosolic release of siRNA.

Lipofection- or polyethylenimine-based siRNA carriers present a substantial toxic effect due to the high density of charge and limited biodegradability of cationic lipids or polymer,[7] and thus such siRNA delivery systems have a limitation to be utilized *in vivo*. However, as shown in Figure 4A, our siRNA/CN complexes did not cause any severe toxicity up to 1 μM, and even at 1.4 μM the siRNA/CN complex showed reasonable *in vitro* cell viability. These results support that our capsid-derived chimeric protein nanoparticles are biocompatible in the cell culture system.

siRNA is an anionic macromolecule that does not readily enter cells by passive diffusion mechanisms, and thus an appropriate siRNA delivery system should enhance its cellular uptake efficiency. With the FITC-labeled siRNA and Cy5.5-labeled capsid nanocarriers, we tracked the internalization of the FITC-siRNA/Cy-5.5-CN complexes in B16F10 melanoma cells. After 1 h of incubation, we clearly noticed siRNAs (green spots) and capsid nanocarriers (red spots) inside the cells (Figure 4B), although whether the siRNAs inside the cells existed as the encapsulated or dissociated forms was not clear. As a control, the FITC-siRNA alone was employed for uptake studies, and its cellular uptake was not observed as we expected (data now shown). Therefore, these results indicate that the encapsulated siRNAs successfully enter the cells through our capsid nanocarrier system. Notably, even at the prolonged incubation time, neither siRNAs nor capsid nanocarriers were seen in the cell nucleus, and this finding indicates that our capsid nanocarriers did not enter the nucleus. In competition experiments using a "cyclic" RGD peptide, preincubation of B16F10 cells with a 100-, 200-, or 400-fold molar excess of cyclic RGD peptides significantly reduced the cell uptake of capsid nanocarriers (Figure 4C). These results can be explained by the competitive binding of cyclic RGD and thus provide evidence that cell uptake of capsid nanocarriers may be mediated by the RGD peptides−integrin interactions.

Generally, the intracellular fate of the macromolecular carriers is strongly affected by the route of entry, and

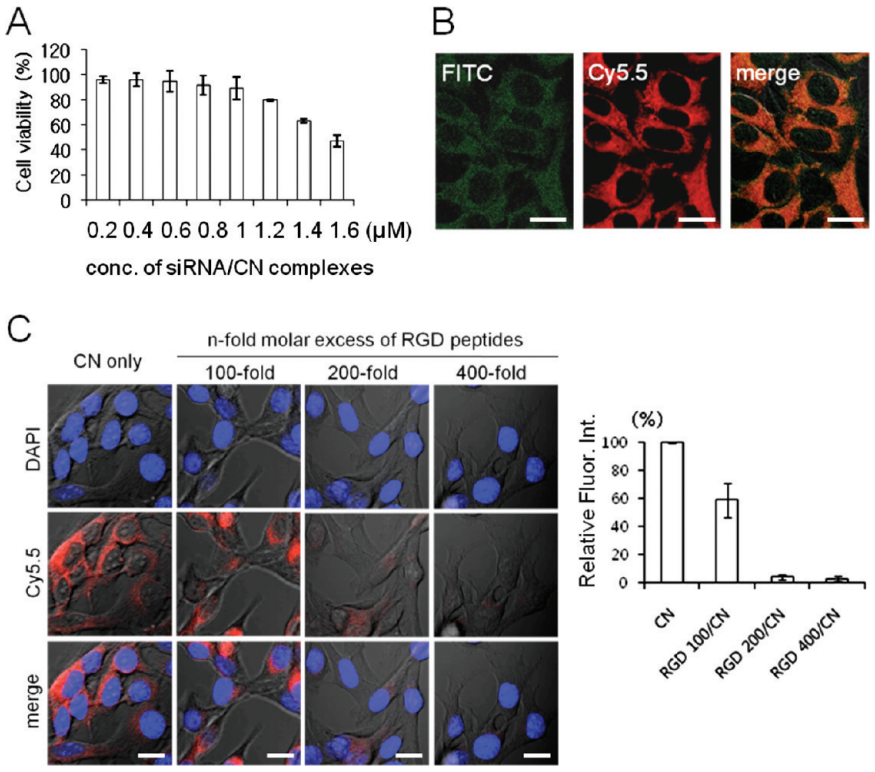

Figure 4. (A) *In vitro* cytotoxicity of RFP/B16F10 cells treated with siRNA/CN complexes was measured by a MTT assay. The results represent the means ± SD (n = 5). (B) Confocal microscopy images of melanoma B16F10 cells (B16F10) after 1 h of incubation with FITC-siRNA/Cy5.5-CN complexes. Green and red signals inside cells represent FITC-labeled siRNA and Cy5.5-labeled capsid nanocarrier, respectively. Scale bar = 10 μm. (C) Competition experiments with cyclic RGD peptides were performed to inhibit the capsid nanocarriers from binding the integrin on cell surface. The B16F10 cells were preincubated with a 100-, 200-, or 400-fold molar excess of cyclic RGD peptides and then treated with Cy5.5-labeled capsid nanocarriers. The fluorescence intensities of the Cy5.5-capsid nanocarriers were quantified and plotted. Each was corrected relative to the value obtained from the image with capsid nanocarrier alone. We tested three different samples per each experiment, and 100 cells/each experiment (total 300 cells) were randomly selected for imaging analysis. Results are presented as mean ± SE (n = 300). Scale bar = 10 μm.

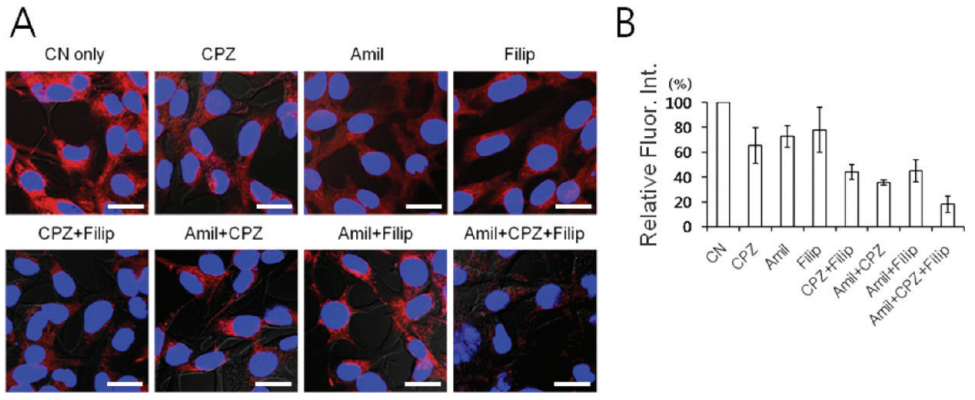

Figure 5. (A) Effects of endocytic inhibitors on internalization of capsid nanocarriers. Prior to treatment of Cy5.5-capsid nanocarriers, B16F10 cell cultures were preincubated with chlorpromazine (CPZ), filipin III (Filip), or amiloride (Amil) in serum-free media for 1 h. The cellular internalization was visualized by a confocal laser scanning microscope. Scale bar = 10 μm. (B) The reduced cell uptake of Cy5.5-capsid nanocarriers was plotted by measuring the fluorescence intensities of the cells. Each was corrected relative to the value obtained from the image with capsid nanocarrier alone. Results are presented as mean ± SE (n = 300).

several endocytic pathways for macromolecules are identified to date: clathrin-mediated endocytosis, caveolae-mediated endocytosis, macropinocytosis, and clathrin- and caveolae-independent endocytosis.[37,38] In an effort to identify the uptake mechanisms involved in the cellular entry of capsid nanocarriers, we employed several endocytic inhibitors, each known to be specific for a particular endocytic pathway. When B16F10 cells were preincubated with CPZ and Filip to identify the uptake mechanism through macropinocytosis, the cell uptake was reduced to approximately 45% compared to that of control cells (Figure 5). However, preincubation with Amil and CPZ, which identifies the uptake mechanism through caveolae-mediated endocytosis, decreased the cell uptake

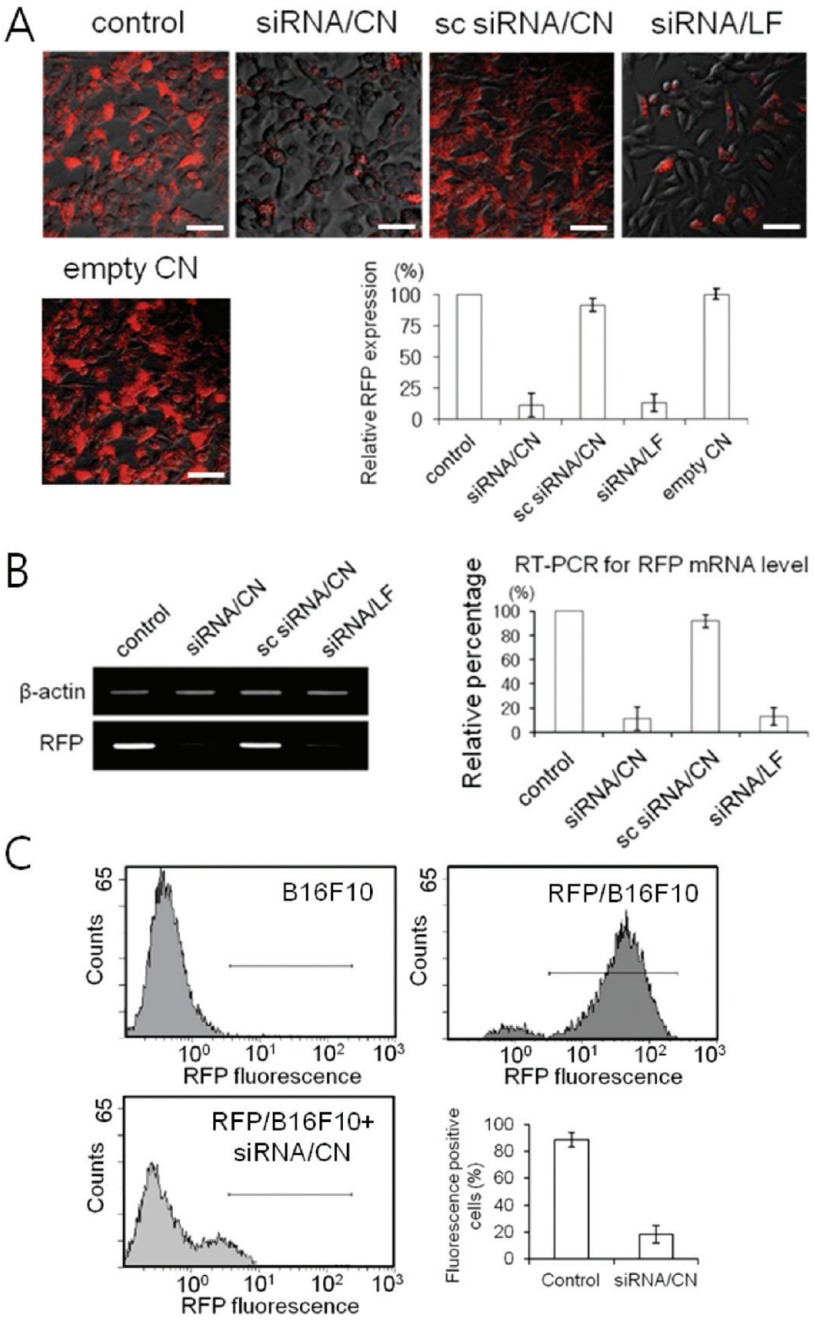

Figure 6. (A) siRNA/CN complexes-mediated RFP gene silencing in RFP/B16F10 cells. Confocal images of the cells were obtained 1 day post-treatment with siRNA/CN complexes (equivalent to 200 nM siRNA). The quantitative analysis of RFP expression was plotted by measuring the fluorescence intensities of the RFP expressed cells. Each measurement was corrected relative to a control. The control cells were treated with PBS buffer, and the results of the scrambled siRNA/CN complexes and empty capsid nanocarriers were also compared. siRNA/Lipofectamine 2000 (siRNA/LF) complexes were prepared according to the manufacturer's protocol. Results are presented as mean ± SE (n = 300). Scale bar = 20 μm. (B) Semiquantitative RT-PCR analysis for RFP mRNA level. The RFP expression reduction was quantified by normalizing with β-actin expression. Results are presented as mean ± SE (n = 5). (C) Representative flow cytometry analysis data are shown for RFP-expressing B16F10 cells either untreated or treated with siRNA/CN complexes. The percentage of RFP positive cells was determined by gating against RFP/B16F10 cells. The fluorescence-positive proportions of untreated and siRNA/CN complexes-treated cells are also compared. Results are presented as mean ± SE (n = 5).

efficacy to approximately 35%. Similarly, preincubation with Amil and Filip, which identifies the uptake mechanism through clathrin-mediated endocytosis, reduced the cell uptake efficacy to approximately 47%. Furthermore, triple-inhibitor studies showed the cell uptake was reduced to 20%. Therefore, our inhibition studies indicate that the internalization of capsid nanocarriers is presumably mediated by more than one cellular uptake mechanism.

With our siRNA/CN complexes, we finally investigated the efficacy of gene silencing in the RFP gene expressing B16F10 cells (RFP/B16F10). One day after treatment, the level of RFP expression was analyzed by

visualizing RFP gene knockdown. As shown in Figure 6A, the fluorescence microscopy images showed that the treatment of siRNA/CN complexes effectively suppressed the expression of RFP in the cells, compared to the control cells. This gene silencing efficacy was similar to that of Lipofectamine 2000 (LF)/siRNA complexes. However, the scrambled siRNA/CN complexes could not suppress the RFP gene expression in the cells. As a negative control, the cells treated with the empty capsid nanocarriers showed RFP gene expression similar to that of the control cells. In the prolonged incubation time, RFP gene silencing by the siRNA/CN complexes was observed until 2 days, but further gene silencing effect was not seen 3 days post treatment. These results indicate that at least for 2 days siRNA delivered by our siRNA/CN complexes system may remain stable in the cells. RT-PCR, which analyzes degradation of the RFP mRNA, also showed the siRNA/CN complexes had a great gene silencing efficacy to RFP gene expression, wherein approximately 90% of RFP gene reduction was observed compared to untreated control cells (Figure 6B). Fluorescence activated cell analysis (FACS) also showed that the RFP fluorescence-positive fraction of B16F10 cells was 88.5 $\pm$ 5.4% in untreated cells but was significantly reduced to 18.5 $\pm$ 6.5% in siRNA/CN-treated cells (Figure 6C). The mean fluorescence intensity was reduced to 20.2 $\pm$ 1.5% in siRNA/CN-treated cells when compared to RFP-expressing B16F10 cells. These results indicate that the siRNA/CN complexes can break down the specific mRNA in the cell culture system.

In conclusion, we synthesized a new siRNA delivery carrier composed of a capsid shell, integrin targeting peptide, and p19 RNA binding protein, by mimicking the gene delivery function of the capsid proteins. Our capsid nanocarriers have two necessary functionalities for siRNA delivery, to encapsulate the siRNA of interest and to be taken up by target cells. The shielding effect derived from the capsid shell structure could enhance stability of the encapsulated siRNA in serum conditions. Also, the RGD peptides on the shell surface allowed the capsid nanocarriers to be recognized by the integrins overexpressed on the cancer cell surface and be subsequently internalized *via* endocytosis pathways.

Notably, our capsid nanocarriers have specificity to siRNA size (*i.e.*, a size range of 20−23 nucleotides) and siRNA shape (*i.e.*, RNA duplex).[32,33] Thus, only double-stranded siRNA with a size range of 20−23 nucleotides can be encapsulated into the interior of capsid nanocarriers, whereas other nucleotides including DNA, single-stranded siRNA, or rRNA cannot be loaded. It was shown experimentally that 34-bp DNA oligonucleotides may be packaged *in vitro* by the natural HBV capsids,[39] which have arginine-rich C-terminal domain required for nucleic acid binding. However, this strategy for encapsulation of oligonucleotides has the limitations that removal of the bacterially originated RNA from the particle interior should be preferentially performed by RNases immediately after the capsids are dissociated into dimers; this approach also requires the reassembling process of the capsids to pack oligonucleotides.

In contrast to the high toxicity of cationic lipids or polymers utilized in siRNA delivery systems, our protein-based capsid nanocarriers did not show any severe cytotoxicity in the cell culture system. Retroviruses are one of the first vectors used to transduce cells with plasmids expressing hairpin-RNA constructs, but when integrating their DNA into the host's genomic DNA, they bring with it the risk of mutagenesis and carcinogenesis.[13] Our capsid nanocarriers mimick the gene delivery function of the virus particles, but they do not have the risk of mutagenesis and carcinogenesis expected in the viral vectors, because our recombinant proteins do not contain the genetic materials for host genome interaction and viral replication cycle. Also, the pH-dependent binding ability of the capsid nanocarriers for siRNA allowed the complexed siRNA to be released into the cytosolic space after cell uptake. Finally, we demonstrated the efficiency of siRNA/CN complexes for both siRNA delivery and RNAi activity through *in vitro* RFP gene silencing.

When a therapeutic siRNA for cancer is encapsulated to the capsid nanocarrier systems, the shielding effect of the capsid structure is expected to enhance the stability of siRNA during body circulation *in vivo*. In addition, the RGD-mediated cellular uptake ability of the capsid nanocarriers may efficiently deliver the therapeutic siRNA to the tumor sites. Besides the RGD peptides, modification of the exterior of the capsid shell (*e.g.*, conjugation with target-specific antibodies or aptamers) would allow the capsid nanocarriers to be specifically delivered to the target sites. In this article, our results provide an alternative approach to enhancing the stability of siRNA as well as to achieving the targeted siRNA delivery and suggest that our capsid nanocarrier system has the potential of the efficient siRNA carrier in the therapeutic applications.

EXPERIMENTAL SECTION

Materials. RFP siRNA and a mismatched scrambled (sc) RFP siRNA for target RFP gene silencing were synthesized and annealed by Bioneer (Daejeon, Korea) with the following sequences; RFP sense strand: 5′-UGUAGAUGGACUUGAACUC-dTdT-3′; RFP antisense strand: 5′-GACUUCAAGUGCAACUUCA-dTdT-3′; sc sense strand: 5′-UGAAGUUGCACUUGAAGUCdTdT-3′; and sc antisense strand: 5′-GACUUCAAGUGCAACUUCAdTdT-3′. FITC-labeled siRNA (the 5′-end of RFP sense strand conjugated with FITC dye) was also purchased from Bioneer. The monoreactive hydroxysuccinimide ester of Cy5.5 (Cy5.5-ester) was from Amersham Biosciences (Piscataway, NJ). Dimethyl sulfoxide (DMSO) and methanol were purchased from Merck (Darmstadt, Germany). Ethidium bromide (EtBr) was obtained from Sigma (St. Louis, MO).

The cyclic RGD peptides with the sequence H-ACRGDMFGCA-OH were synthesized by Peptron (Daejeon, Korea). Lipofectamine2000 was purchased from Invitrogen. Chlorpromazine hydrochloride, filipin III, and amiloride hydrochloride hydrate were purchased from Sigma. All other chemicals were purchased as reagent grade and used without further purification. All solution were made up in RNase-free distilled water and autoclaved prior to use. The Pymol program (version 1.4.1) for 3D structural analysis of capsid architecture was obtained from DeLano Scientific LLC.

Biosynthesis and Purification of Capsid-p19 Fusion Protein. Following PCR amplification with appropriate primers, we prepared two amplified products for the truncated capsid fragment (1−149 aa) derived from the HBV core protein (HBVcAg) gene and full-length p19 RNA binding protein gene derived from Carnation Italian ringspot virus (CIRV), respectively. Next, the overlap extension polymerase chain reaction method[40] was utilized to splice two DNA sequences (corresponding to the capsid fragment and p19 protein, respectively), wherein the linker gene (corresponding to the 31-mer peptide GSSGGSGSSGGSGGGDEADGSRGSQKAGVDE) was incorporated to be located between two DNA sequences. Through restriction enzyme cutting and sequential ligation of the gene into plasmid pET-28a(+), we prepared the capsid-p19 fusion gene clone. To incorporate RGD peptides to the fusion protein, we replaced A80 and S81 of the capsid fragment with the RGD4C peptide (CDCRGDCFC) by using a QuickChange Site-Directed Mutagenesis kit (Stratagene). After the complete DNA sequencing of the gel-purified plasmid expression vector, *E. coli* strain BL21(DE3) was transformed with the pET-28a(+)/capsid-p19 vector, and kanamycin-resistant transformants were selected.

For gene expression of the capsid-p19 fusion protein, cells were grown until OD_{600} of 0.5 in LB medium containing 50 mg/mL kanamycin, and then protein expression was induced by 1.0 mM isopropyl-β-D-thiogalactopyranoside (IPTG). After 18 h of further growth, the cells were harvested, and then the resulting cell pellet was resuspended in the lysis buffer (50 mM Tris-HCl pH 8.0, 100 mM sodium chloride, 1 mM phenylmethylsulfonyl fluoride). Using an ultrasonic processor, the cells were lysed, and the soluble fractions were purified with two chromatographic steps: the first step was performed by metal-chelate chromatography using Ni-NTA resin (Qiagen), and then the proteins were further purified by size exclusion chromatography (SEC) using a Superdex 200 10/300 GL column (GE Healthcare), previously equilibrated with a buffer containing 50 mM Tris-HCl (pH 8.0), 100 mM sodium chloride, and 1 mM mercaptoethanol.[31] The homogeneity of the purified protein was assessed by SDS-PAGE,[41] and the protein concentration was calculated by a Bradford assay with bovine serum albumin as a standard.[42] The protein solution was concentrated using an YM10 ultrafiltration membrane (Amicon). To analyze the assembled structure of the capsid protein, a standard protein curve on the size exclusion chromatography was prepared; 24-mer of wild-type ferritin (M_r 440 kDa), BSA (M_r 67 kDa), and cytochrome *c* (M_r 14 kDa) were eluted at V_e = 9−10, 15−16, and 20−21 mL, respectively. After purification steps, a protein yield of the capsid nanocarriers was estimated as 2.5 mg/L in LB medium, whereas that of the native capsid proteins was 4.5 mg/L.

Labeling of Capsid Nanocarriers with Cy5.5 Dyes. NIR fluorescence Cy5.5 dyes with the NHS ester group were conjugated to the amine groups (-NH_2) of lysine residues on the exterior surface of the capsid nanocarriers (CN) to track their cellular internalization in cell culture system. The conjugation reaction was stirred at room temperature for 2 h while protected from light. To remove the unbound Cy5.5 dyes from the capsid nanocarriers, the reaction mixture was injected into a size exclusion column, which simultaneously could monitor UV absorbance by the protein sample at 280 nm and NIRF from Cy5.5 molecules at 674 nm, respectively. When compared to the standard protein curve, the Cy5.5-capsid nanocarriers were eluted as a single peak at an elution volume corresponding to that of the self-assembled native capsid particles. These results indicated that the assembled capsid structure did not change during the Cy5.5 conjugation process. Moreover, the fluorescence signal from Cy5.5 dyes coincided with an elution peak of the capsid nanocarriers, and these results revealed that the Cy5.5 dyes were covalently bonded to the capsid nanocarriers.

Encapsulation of siRNA and Characterization of Capsid Nanocarriers. The FITC-labeled siRNA (20 μg) in RNase-free distilled water (200 μL) was complexed with various amounts of capsid nanocarriers, at a molar ratio from 4 to 240 (siRNA per capsid nanocarrier). After incubation in the PBS buffer (pH 7.4) for 1 h at room temperature, the complex formation was confirmed by a gel retardation assay (20% polyacylamide gel) in the Tris/Borate/EDTA (TBE) buffer. The bands on the gel were visualized by a 12 bit CCD camera (KODAK Image Station 4000MM, Japan) equipped with a special C mount lens and FITC bandpass emission filter (Omega Optical; 488−530 nm).

To examine whether siRNAs were encapsulated into the interior of capsid nanocarriers, the capsid nanocarriers were complexed with the FITC-labeled siRNA and subsequently injected into a SEC column (a Superdex 200 10/300 GL). The peak fractions corresponding to the high molecular weight of the capsid assembly were analyzed by a F-7000 fluorescence spectrophotometer (Hitachi, Jappan). The emission spectra of the pooled fractions were scanned at a fixed excitation wavelength (λ_{ex} = 488 nm). Also, the emission spectrum of the capsid nanocarrier alone was compared with that of siRNA/capsid nanocarrier complexes. As a positive control, the emission spectra of the fluorescent FITC dye were scanned at two different concentrations.

To determine the amount of siRNA in the siRNA/CN complexes, 1 mL of TRIZOL was added to the peak fractions of the SEC column and briefly vortexed. Then, 0.3 mL of cold chloroform was added and vortexed. The resulting solution was centrifuged at 12,000 rpm for 15 min. The upper aqueous phase was removed, an equivalent volume of isopropyl alcohol, about 0.5 mL, was added, and then the tube was placed in a freezer at −20 °C for 10 min. After centrifugation at 12,000 rpm for 15 min, the supernatant was removed, and the pellet was resuspended in 0.4 mL of DEPC water. Next, 0.4 mL of cold phenol/chloroform was added, and the tube was centrifuged at 12,000 rpm at 4 °C for 15 min. The upper phase was removed, and 37 μL of 3 M sodium acetate and 800 μL of 100% ethanol were added. After centrifugation at 14,000 rpm at 4 °C for 30 min, the supernatant was removed, and the pellet was washed with 75% ethanol. Another cenrifugation was performed at 14,000 rpm at 4 °C for 30 min, and the supernatant was removed. After the tube was dried for 5 min, the pellet was resuspended in 200 μL of DEPC water. The concentration of siRNA was measured at A_{260} by spectrophotometry.

For the particle size and morphology measurement, dynamic light scattering (DLS) measurement was conducted at 633 nm and 25 °C using a model 127-35 laser (Spectra Physics). We used a CM30 electron microscope (Philips) for transmission electron microscopy (TEM) images, operating at an acceleration voltage of 80 kV. In the TEM measurement, a drop of sample solution (1 mg/mL) was placed onto a 300-mesh copper grid coated with carbon. Approximately 2 min after deposition, the grid was tapped with filter paper to remove surface water and then air-dried. Negative staining was performed using a droplet of a 2 wt % aqueous uranyl acetate solution.

siRNA Stability Test and pH-Dependent Complexing of Capsid Nanocarriers with siRNA. The free siRNA or siRNA/CN complexes containing 0.2 μg of siRNA were incubated with RNases present in 50% fetal bovine serum (FBS) at 37 °C for up to 96 h. The incubation experiments were performed in PBS conditions (pH 7.4). According to the incubation times, aliquots from each sample were electrophoresed on 20% polyacylamide gel in the TBE buffer. Under the electrophoresis condition, the siRNA encapsulated by the capsid shell remained in the loading wells, but the free siRNA entered the gel and ran as a clearly visible band. The FITC-labeled siRNA was used to enhance the detection limit and its fluorescent images were obtained by Kodak Image Station.

In the various pH conditions, dissociation of siRNA from the siRNA/CN complexes was examined by the gel electrophoresis. The siRNA/CN complexes were incubated in the indicated pH conditions ranging from 7.4 to 5.0 for 15 min at room temperature, and then each sample were electrophoresed on 20%

polyacylamide gel. The media conditions for each pH are as follows: pH = 7.4 (PBS buffer (7.4)), pH = 6.5 (20 mM sodium phosphate buffer (6.5), 100 mM NaCl), pH = 6.0 (20 mM sodium phosphate buffer (6.0), 100 mM NaCl), pH = 5.5 (20 mM sodium acetate buffer (5.5), 100 mM NaCl), and pH = 5.0 (20 mM sodium acetate buffer (5.0), 100 mM NaCl). The encapsulated or dissociated siRNA was visualized by EtBr staining under UV light. The bands were observed by Minibis Bioimaging system (DNR Bio-Imaging Systems Ltd., Israel) and quantified by GelQuant software.

MTT Assay and Cellular Uptake Studies. *In vitro* cytotoxicity of siRNA/CN complexes was studied in the red fluorescent protein (RFP) gene expressing murine melanoma cell (RFP/B16F10) culture system. Briefly, RFP/B16F10 cells were seeded on a 96-well plate at a cell density of 1×10^4 cells/mL and allowed to grow for 24 h in RPMI1640 with 10% FBS. Cells were then transfected with 0.2−1.6 μM siRNA/CN complexes per well. After 24 h of incubation, 200 μL of MTT (0.5 mg/mL) dissolved in the PBS buffer was added to each well, and the cells were incubated for 4 h to produce formazan crystals. The formazan crystals were subsequently dissolved in 200 μL of DMSO and 25 μL of Sorensen's glycine buffer, and then their quantity was measured at 570 nm by a microplate reader (Spectra max340, Molecular Device, CA). The absorbance of the nontransfected cells was used as a control, and each absorbance was corrected relative the control value. To examine the cytotoxicity of the siRNA/CN complexes for the relatively small time range, the cells were incubated with the siRNA/CN complexes for 12 h, and then their cell viability was evaluated in a similar manner. In both cytotoxicity studies, there was no remarkable difference in the cell viabilities.

With the FITC-labeled siRNA and Cy5.5-labeled capsid nanocarriers, we tracked the cellular internalization of either siRNAs or capsid nanocarriers in murine melanoma cells (B16F10). After siRNA/CN complexes treatments (10 μg/mL), the cells were washed twice with PBS containing Mg^{2+} and Ca^{2+} and then fixed with formaldehyde/glutaraldehyde-combined fixative for 15 min. The fluorescence images were obtained by a FV1000 confocal laser scanning microscope (Olympus) equipped with argon (488 nm) and HeNe (543 nm) lasers. Cross-talk between FITC and Cy5.5 signal channels was removed by using Line Sequential Action software.

In the competition experiment using cyclic RGD peptides, the B16F10 cells were preincubated with a 100-, 200-, or 400-fold molar excess of cyclic RGD peptides for 1 h, and then the cellular internalization of the Cy5.5-labeled capsid nanocarriers was examined by a confocal laser scanning microscope. The sequence of the cyclic RGD peptides was derived from the integrin-binding RGD peptides indentified by phage display and has been found effective for cell binding and internalization.[29]

The effects of several membrane entry inhibitors on the capsid nanocarrier's uptake were examined by incubating the B16F10 cell cultures with chlorpromazine (10 μg/mL) to inhibit the formation of clathrin vesicles, filipin III (1 μg/mL) to inhibit caveolae, or amiloride (50 μM) to inhibit macropinocytosis. Chlorpromazine (CPZ) dissociates clathrin from the surface membrane to inhibit the clathrin-mediated endocytosis.[43] Filipin III (Filip) inhibits the caveolae-mediated endocytosis by blocking of caveolae formation.[44] Amiloride (Amil) inhibits the macropinocytosis by blocking the Na^+/H^+ exchange required for macropinocytosis.[45] Because the capsid nanocarriers were labeled with the fluorescent Cy5.5 dyes, their cellular internalization could be visualized under a confocal laser scanning microscope. The nucleus in each cell was stained with DAPI (blue) following the supplier's protocol. The statistical analysis was carried out using ASW2.0c software. Statistical analysis for the quantification approach was carried out using one-way ANOVA, and the results were reported as mean ± SD. In all cases, $p < 0.05$ was considered significant.

RFP Gene Silencing in Cell Culture System and RT-PCR. *In vitro* gene silencing efficacy of siRNA/CN complexes was evaluated with RFP gene expressing B16F10 cells. The cells were plated at a density of 1×10^4/well in slideglass bottomed 35 mm culture dishes. After 24 h of incubation, cell culture media were replaced with serum-free transfection media, and siRNA/CN complexes or scrambled siRNA/CN complexes (equivalent to 200 nM siRNA) were treated to the cells for 4 h. As a positive control for gene silencing test, siRNA/Lipofectamine 2000 (siRNA/LF) complexes were prepared according to the manufacturer's protocol. After 4 h treatments, transfection media were removed and replaced with fresh RPMI media containing 10% FBS, and then the cells were further incubated for 20 h at 37 °C. After the cells were fixed, we observed RFP signals of each sample using a confocal laser scanning microscope. For RFP fluorescent imaging, autofluorescence originally emitted in B16F10 cells was examined and could be removed by precisely controlling laser intensities. Offset action software equipped in a confocal microscope allowed the background signals to be removed.

Also, we performed reverse transcription-polymerase chain reaction (RT-PCR) to analyze the RFP gene silencing efficacy of siRNA/CN complexes in the RFP/B16F10 cell culture system. After 24 h post incubation, the cells were harvested and lysed, and total RNAs were extracted by using a RNeasy mini kit (QIAGEN, Valencia, CA), according to the manufacturer's protocol. The residual DNA was removed by on-column DNase digestion using the RNase-Free DNase Set, and the DNase was efficiently removed in subsequent wash steps. A_{260}/A_{280} ratio of the extracted RNA was 1.86, and the RNA was expected to be of sufficient quality and suitable for RT-PCR application. Reverse transcription was performed by MultiScribe Reverse Transcriptase contained in the High-capacity cDNA Reverse Transcription Kits (Applied Biosystems, Foster city, CA). The PCR primers (for β-actin: forward 5′-AGAGGGAAATCGTGCGTGAC-3′, reverse 5′-CAATAGTGATGACCTGGCCGT-3′, for RFP: forward 5′-GGCTG-CTTCATCTACAAGGT-3′, reverse 5′-GCGTCCACGTAGTAGTAG-CC-3′) were synthesized and purified by Bioneer (Daejeon, Korea). Twenty nanograms of cDNA per reaction was amplified during 20 cycles using the primers. The sizes of the PCR-amplified products were 138 and 245 bp, respectively, and they were separated in 2% agarose gel electrophoresis. The relative expression levels of RFP gene were normalized against expression of the β-actin gene and quantified by TINA Image analysis software. When the extracted RNA was incubated without reverse transcriptase and subsequently amplified *via* PCR, PCR-amplified product was not detected on 2% agarose gel. The relative expression level of RFP gene was presented as mean ± SE ($n = 3$). Also, RFP expression was assessed using fluorescence activated cell analysis (FACS) (FC-500 flow cytometer, Beckman Coulter, Miami, FL). Ten thousand cells were investigated for RFP expression by FACS, and cells were detached from plates with trypsin-ethylenediamine tetraacetic acid.

Acknowledgment. This research was supported by the Converging Research Center Program through the Ministry of Education, Science and Technology (2010K001205) and by the National Research Foundation of Korea (NRF) grant funded by the Korea government (MEST) (2010-0029206).

REFERENCES AND NOTES

1. Dykxhoorn, D. M.; Lieberman, J. Running Interference: Prospects and Obstacles to Using Small Interfering RNAs as Small Molecule Drugs. *Annu. Rev. Biomed. Eng.* **2006**, *8*, 377–402.
2. Martinez, J.; Patkaniowska, A.; Urlaub, H.; Luhrmann, R.; Tuschi, T. Single-Stranded Antisense siRNAs Guide Target RNA Cleavage in RNAi. *Cell* **2002**, *110*, 563–574.
3. Elbashir, S. M.; Harborth, J.; Lendeckel, W.; Yalcin, A.; Weber, K.; Tuschi, T. Duplexes of 21-Nucleotide RNAs Mediate RNA Interference in Cultured Mammalian Cells. *Nature* **2001**, *411*, 494–498.
4. Iorns, E.; Lord, C. J.; Turner, N.; Ashworth, A. Utilizing RNA Interference to Enhance Cancer Drug Discovery. *Nat. Rev. Drug Discovery* **2007**, *6*, 556–568.
5. Lu, P. Y.; Xie, F.; Woodle, M. C. *In vivo* Application of RNA Interference: from Functional Genomics to Therapeutics. *Adv. Genet.* **2005**, *54*, 117–142.

6. Oishi, M.; Nagasaki, Y.; Itaka, K.; Nishiyama, N.; Kataoka, K. Lactosylated Poly(ethylene glycol)-siRNA Conjugate through Acid-Labile Beta-Thiopropionate Linkage to Construct pH-Sensitive Polyion Complex Micelles Achieving Enhanced Gene Silencing in Hepatoma Cells. *J. Am. Chem. Soc.* **2005**, *127*, 1624–1625.
7. Shim, M. S.; Kwon, Y. J. Efficient and Targeted Delivery of siRNA *In Vivo*. *FEBS J.* **2010**, *277*, 4814–4827.
8. Brummelkamp, T. R.; Bernards, R.; Agami, R. Stable Suppression of Tumorigenicity by Virus-Mediated RNA Interference. *Cancer Cell* **2002**, *2*, 243–247.
9. Zhang, S.; Zhao, B.; Jiang, H.; Wang, B.; Ma, B. Cationic Lipids and Polymers Mediated Vectors for Delivery of siRNA. *J. Controlled Release* **2007**, *123*, 1–10.
10. Sabbioni, S.; Callegari, E.; Manservigi, M.; Argnani, R.; Corallini, A.; Negrini, M.; Manservigi, R. Use of Herpes Simplex Virus Type 1-Based Amplicon Vector for Delivery of Small Interfering RNA. *Gene Ther.* **2007**, *14*, 459–464.
11. Makinen, P. I.; Koponen, J. K.; Karkkainen, A. M.; Malm, T. M.; Pulkkinen, K. H.; Koistinaho, J.; Turunen, M. P.; Yla-Herttuala, S. Stable RNA Interference: Comparison of U6 and H1 Promoters in Endothelial Cells and in Mouse Brain. *J. Gene Med.* **2006**, *8*, 433–441.
12. Wadhwa, R.; Kaul, S. C.; Miyagishi, M.; Taira, K. Vectors for RNA Interference. *Curr. Opin. Mol. Ther.* **2004**, *6*, 367–372.
13. Tomaini, R.; Scarpa, M. Why Do We Need New Gene Therapy Viral Vectors? Characteristics, Limitations and Future Perspectives of Viral Vector Transduction. *Curr. Gene Ther.* **2004**, *4*, 357–372.
14. Devroe, E.; Silver, P. A. Therapeutic Potential of Retroviral RNAi Vectors. *Expert Opin. Biol. Ther.* **2004**, *4*, 319–327.
15. Layzer, J. M.; McCaffrey, A. P.; Tanner, A. K.; Huang, Z.; Kay, M. A.; Sullenger, B. A. *In Vivo* Activity of Nuclease-Resistant siRNAs. *RNA* **2004**, *10*, 766–771.
16. Zhang, S.; Zhao, B.; Jiang, H.; Wang, B.; Ma, B. Cationic Lipids and Polymers Mediated Vectors for Delivery of siRNA. *J. Controlled Release* **2007**, *123*, 1–10.
17. Tan, P. H.; Yang, L. C.; Shih, H. C.; Lan, K. C.; Cheng, J. T. Gene Knockdown with Intrathecal siRNA of NMDA Receptor NR2B Subunit Reduces Formalin-Induced Nociception in the Rat. *Gene Ther.* **2005**, *12*, 59–66.
18. Thomas, M.; Lu, J. J.; Ge, Q.; Zhang, C.; Chen, J.; Klibanov, A. M. Full Deacylation of Polyethylenimine Dramatically Boosts Its Gene Delivery Efficiency and Specificity to Mouse Lung. *Proc. Natl. Acad. Sci. U.S.A.* **2005**, *102*, 5679–5684.
19. Watanabe, K.; Harada-shiba, M.; Suzuki, A.; Gokuden, R.; Kurihara, R.; Sugao, Y.; Mori, T.; Katayama, Y.; Niidome, T. *In Vivo* siRNA Delivery with Dendritic Poly(L-lysine) for the Treatment of Hypercholesterolemia. *Mol. BioSyst.* **2009**, *5*, 1306–1310.
20. Vangasseri, D. P.; Han, S. J.; Huang, L. Lipid-Protamine-DNA-Mediated Antigen Delivery. *Curr. Drug Delivery* **2005**, *2*, 401–406.
21. Choi, Y. S.; Lee, J. Y.; Suh, J. S.; Kwon, Y. M.; Lee, S. J.; Chung, J. K.; Lee, D. S.; Yang, V. C.; Chung, C. P.; Park, Y. J. The Systemic Delivery of siRNAs by a Cell Penetrating Peptide, Low Molecular Weight Protamine. *Biomaterials* **2010**, *31*, 1429–1443.
22. Akhtar, S.; Benter, I. F. Nonviral Delivery of Synthetic siRNAs *In Vivo*. *J. Clin. Invest.* **2007**, *117*, 3623–3632.
23. Park, T. G.; Jeong, J. H.; Kim, S. W. Current Status of Polymeric Gene Delivery Systems. *Adv. Drug Delivery Rev.* **2006**, *58*, 467–486.
24. Moghimi, S. M.; Symonds, P.; Murray, J. C.; Hunter, A. C.; Debska, G.; Szewczyk, A. A Two-Stage Poly(ethylenimine)-Mediated Cytotoxicity: Implications for Gene Transfer/Therapy. *Mol. Ther.* **2005**, *11*, 990–995.
25. Symonds, P.; Murray, J. C.; Hunter, A. C.; Debska, G.; Szewczyk, A.; Moghini, S. M. Low and High Molecular Weight Poly(L-lysine)s/Poly(L-lysine)-DNA Complexes Initiate Mitochondrial-Mediated Apoptosis Differently. *FEBS Lett.* **2005**, *579*, 6191–6198.
26. Chiu, Y. L.; Rana, T. M. siRNA Function in RNAi: A Chemical Modification Analysis. *RNA* **2003**, *9*, 1034–1048.
27. Czauderna, F.; Fechtner, M.; Dames, S.; Aygun, H.; Klippel, A.; Pronk, G. J.; Giese, K.; Kaufmann, J. Structural Variations and Stabilising Modifications of Synthetic siRNAs in Mammalian Cells. *Nucleic Acids Res.* **2003**, *31*, 2705–2716.
28. Hall, A. H.; Wan, J.; Shaughnessy, E. E.; Ramsay Shaw, B.; Alexander, K. A. RNA Interference Using Boranophosphate siRNAs: Structure-Activity Relationships. *Nucleic Acids Res.* **2004**, *32*, 5991–6000.
29. Schiffelers, R. M.; Ansari, A.; Xu, J.; Zhou, Q.; Tang, Q.; Storm, G.; Molema, G.; Lu, P. Y.; Scaria, P. V.; Woodle, M. C. Cancer siRNA Therapy by Tumor Selective Delivery with Ligand-Targeted Sterically Stabilized Nanoparticle. *Nucleic Acids Res.* **2004**, *32*, e149.
30. Bottcher, B.; Wynne, S. A.; Crowther, R. A. Determination of the Fold of the Core Protein of Hepatitis B Virus by Electron Cryomicroscopy. *Nature* **1997**, *386*, 88–91.
31. Park, J. S.; Cho, M. K.; Lee, E. J.; Ahn, K. Y.; Lee, K. E.; Jung, J. H.; Cho, Y.; Han, S. S.; Kim, Y. K.; Lee, J. A Highly Sensitive and Selective Diagnostic Assay Based on Virus Nanoparticles. *Nat. Nanotechnol.* **2009**, *4*, 259–264.
32. Vargason, J. M.; Szittya, G.; Burgyan, J.; Hall, T. M. Size Selective Recognition of siRNA by an RNA Silencing Suppressor. *Cell* **2003**, *115*, 799–811.
33. Ye, K.; Malinina, L.; Patel, D. J. Recognition of Small Interfering RNA by a Viral Suppressor of RNA Silencing. *Nature* **2003**, *426*, 874–878.
34. Crowther, R. A.; Kiselev, N. A.; Bottcher, B.; Berriman, J. A.; Borisova, G. P.; Ose, V.; Pumpens, P. Three-Dimensional Structure of Hepatitis B Virus Core Particles Determined by Electron Cryomicroscopy. *Cell* **1994**, *77*, 943–950.
35. Whitehead, K. A.; Langer, R.; Anderson, D. G. Knocking Down Barriers: Advances in siRNA Delivery. *Nat. Rev. Drug Discovery* **2009**, *8*, 129–138.
36. Putnam, D.; Gentry, C. A.; Pack, D. W.; Langer, R. Polymer-Based Gene Delivery with Low Cytotoxicity by a Unique Balance of Side-Chain Termini. *Proc. Natl. Acad. Sci. U.S.A.* **2001**, *98*, 1200–1205.
37. Khalil, I. A.; Koqure, K.; Akita, H.; Harashima, H. Uptake Pathways and Subsequent Intracellular Trafficking in Nonviral Gene Delivery. *Pharmacol. Rev.* **2006**, *58*, 32–45.
38. Johannes, L.; Lamaze, C. Clathrin-Dependent or Not: Is It Still the Question? *Traffic* 2002, 3, 443–451.
39. Cooper, A.; Shaul, Y. Recombinant Viral Capsids as an Efficient Vehicle of Oligonucleotide Delivery into Cells. *Biochem. Biophys. Res. Commun.* **2005**, *327*, 1094–1099.
40. Urban, A.; Neukirchen, S.; Jaeger, K. E. A Rapid and Efficient Method for Site-Directed Mutagenesis Using One-Step Overlap Extension PCR. *Nucleic Acids Res.* **1997**, *25*, 2227–2228.
41. Laemmli, U. K. Cleavage of Structural Proteins during the Assembly of the Head of Bacteriophage T4. *Nature* **1970**, *227*, 680–685.
42. Bradford, M. M. A Rapid and Sensitive Method for the Quantitation of Microgram Quantities of Protein Utilizing the Principle of Protein-Dye Binding. *Anal. Biochem.* **1976**, *72*, 248–254.
43. Wang, L. H.; Rothberg, K. G.; Anderson, R. G. Mis-Assembly of Clathrin Lattices on Endosomes Reveals a Regulatory Switch for Coated Pit Formation. *J. Cell Biol.* **1993**, *123*, 1107–1117.
44. Lanaze, C.; Schmid, S. L. The Emergence of Clathrin-Independent Pinocytic Pathways. *Curr. Opin. Cell Biol.* **1995**, *7*, 573–580.
45. Hewlett, L. J.; Prescott, A. R.; Watts., C. The Coated Pit and Macropinocytic Pathways Serve Distinct Endosome Populations. *J. Cell Biol.* **1994**, *124*, 689–703.